JOURNAL OF MATERIALS SCIENCE 17 (1982) 2365–2370

# Formation and magnetic properties of Fe–B–Si metallic glasses

NICHOLAS DECRISTOFARO, ALFRED FREILICH
*Metglas Products Department, Allied Corporation, Parsippany, New Jersey 07054, USA*
GORDON FISH
*Materials Laboratory, Allied Corporation, Morristown, New Jersey 07960, USA*

The equilibrium solidification behaviour of Fe-rich Fe–B–Si alloys has been characterized in terms of primary and secondary crystallization, and correlated to metallic glass formation and properties. A eutectic trough extends from the binary eutectic on the Fe–B edge of the ternary composition diagram toward the binary eutectic on the Fe–Si edge. Metallic glass forming compositions closely follow the path of the eutectic trough, extending from the Fe–B edge to compositions containing approximately 20 at % Si. The relative ease of glass formation and the thermal stability of the glassy state are maximized at compositions along the eutectic trough. The magnetic coercive forces of both as-cast and annealed metallic glasses are minimized along the eutectic trough.

## 1. Introduction

Iron base metallic glasses have been the focus of intensive research because of their high magnetic inductions, soft magnetic properties and potentially low raw materials costs. Of particular interest are glassy Fe–B and Fe–B–Si alloys [1–5]. When employed in transformer cores, these materials exhibit extremely low core losses relative to those of grain oriented silicon steels [6–8].

Many of the thermal and magnetic properties of Fe–B–Si metallic glasses have been documented. However, the equilibrium solidification behaviour of the system remains largely undefined. In this paper, the equilibrium solidification of Fe-rich Fe–B–Si alloys is characterized. The compositional dependence of glass formation, thermal stability, Curie temperature and coercive force of Fe–B–Si metallic glasses are reported and correlated to the equilibrium solidification.

## 2. Experimental procedures

Continuous ribbons of metallic glass alloys were produced by rapid quenching from the melt onto a rotating chill block. Ribbon thickness was varied from 20 to 62 $\mu$m; widths ranged from 6 to 25 mm. Atomic structures of both rapidly quenched ribbon and slowly cooled, equilibrium samples were adjudged by X-ray diffraction.

The crystallization behaviours of the metallic glasses were monitored on a DuPont 990 differential scanning calorimeter (DSC) at 20 and 5° C $min^{-1}$ heating rates. The onset of crystallization was measured as the intercept of the extrapolations of the baseline and the highest crystallization rate portion of the exothermic peak. Melting and solidification temperatures were measured on DuPont 990 and Metler TA-1 differential thermal analysers (DTA) at 20° C $min^{-1}$ heating and cooling rates. Curie temperature measurements were performed on the DSC and a vibrating sample magnetometer.

Relative ductility of a metallic glass sample was measured by bending a loop of ribbon between the platens of a micrometer. The loop radius, $R(\simeq \frac{1}{2}$ the platen spacing) at failure can be converted to a failure strain, $\epsilon$, by the equation $\epsilon = t/2R$ where $t$ is the ribbon thickness.

## 3. Equilibrium solidification behaviour

Equilibrium solidification of Fe-rich Fe–B–Si alloys initiates with primary crystallization just below the liquidus boundary. At low metalloid

0022–2461/82/082365–06$03.22/0  

contents, corresponding to hypoeutectic compositions, primary body centred cubic (bcc) $\alpha$-(Fe, Si) solidifies into a branched dendritic structure. When primary $\alpha$ occupies a large volume fraction, the dendrites degenerate to rounded knobbly shapes as in Fig. 1a. The dark background region is a lamellar eutectic of $\alpha$-(Fe, Si) and $Fe_2B$. This results from secondary solidification of the eutectic liquid at the solidus temperature and is present in all Fe–B–Si compositions studied here. As the metalloid content is increased, the liquidus temperature and volume fraction of primary $\alpha$ both decrease while the dendritic nature of this phase becomes more apparent (Fig. 1b).

At high metalloid contents, corresponding to hypereutectic compositions, $Fe_2B$ is the product of primary solidification. This phase crystallizes into plate-like particles with sharp angular corners, as illustrated in Fig. 1c. The faceted boride morphology is characteristic of a crystal with high anisotropic interfacial energies. In the high metalloid content region, the liquidus temperature and volume fraction of primary $Fe_2B$ increase with increasing metalloid content.

Eutectic crystallization takes place where the downward sloping $L \rightarrow \alpha + L$ and $L \rightarrow Fe_2B + L$ liquidus surfaces meet. The eutectic temperature is approximately 1170° C as determined by continuous heating DTA at 20° C $min^{-1}$. At the eutectic composition, $\alpha$ and $Fe_2B$ precipitate simultaneously from the melt to form a 100% lamellar eutectic microstructure, as in Fig. 1d. The line of intersection of the two liquidus surfaces is charted on the ternary composition diagram of Fig. 2. This eutectic trough extends from the binary eutectic on the Fe–B edge towards the binary eutectic on the Fe–Si edge. At Si contents greater than about 20 at%, additional Fe–Si and Fe–B–Si phases precipitate from the melt. From this point to the Fe–Si edge (dashed portion of the line), the solidification reaction becomes more complex.

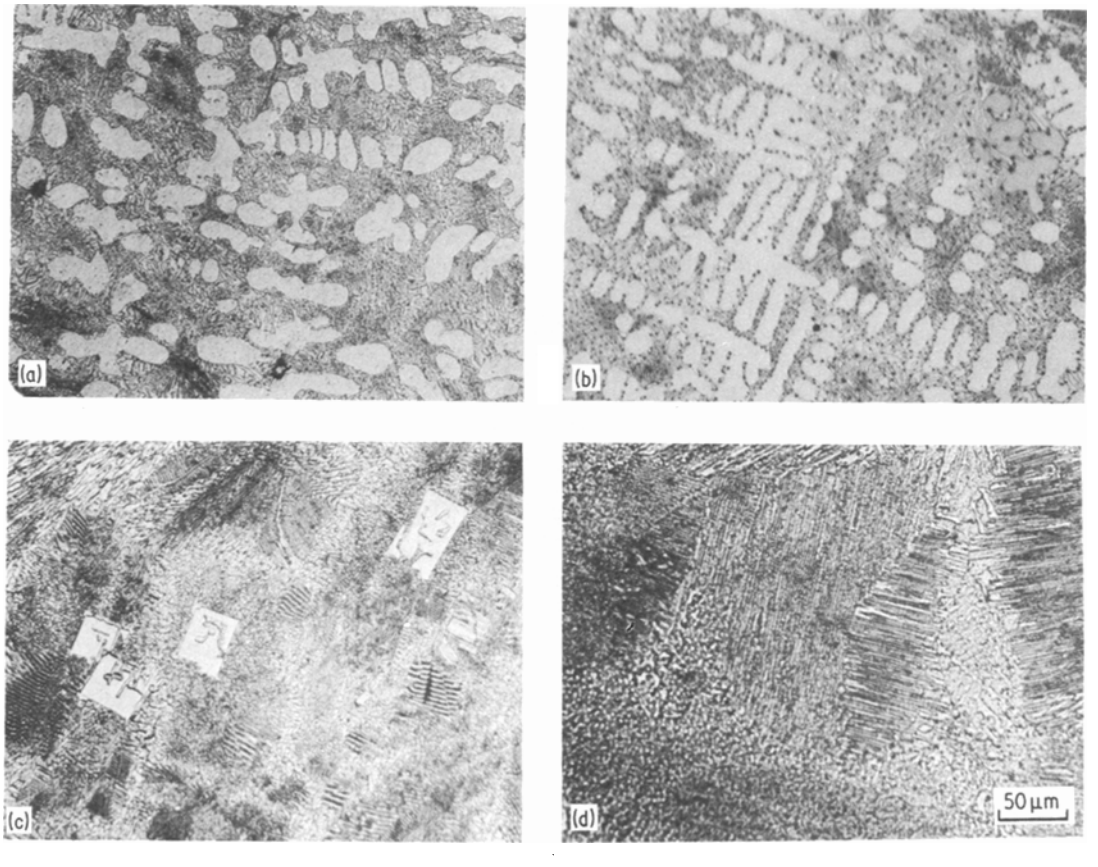


*Figure 1* Microstructures of equilibrium solidified Fe–B–Si alloys: (a) $Fe_{84}B_8Si_8$ (b) $Fe_{80}B_{10}Si_{10}$ (c) $Fe_{78}B_{14}Si_8$ and (d) $Fe_{82}B_{15}Si_3$ etched in 10% Nital.

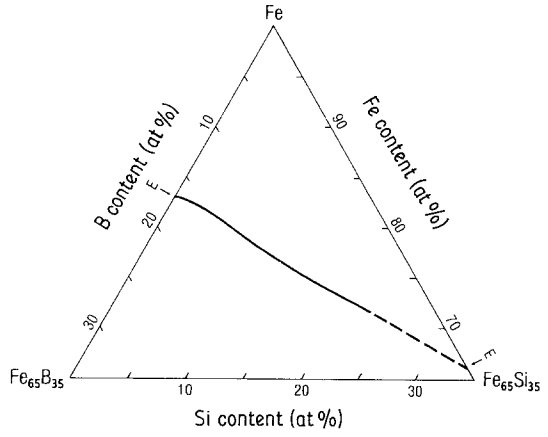


*Figure 2* The eutectic trough [L → α-(Fe, Si) + $Fe_2B$] for slowly cooled Fe–B–Si alloys.

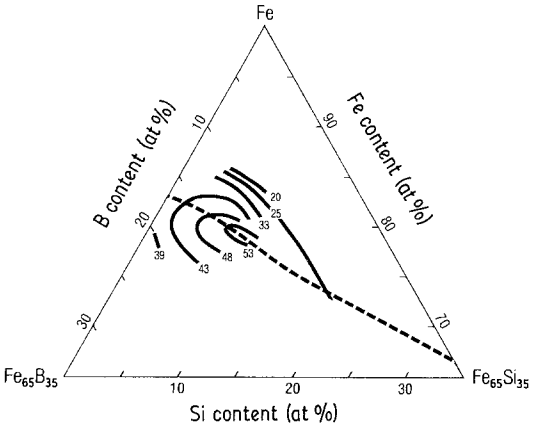


*Figure 4* Contours of maximum ribbon thickness, in μm, consistent with $\epsilon = 1$ bend ductility. The eutectic trough is marked by the dashed ( – – – ) line.

## 4. Glass forming compositions

The glass forming region in the Fe–B–Si ternary system is outlined in Fig. 3. This area closely follows the course of the eutectic trough across the ternary diagram, extending from the binary Fe–B edge to ternary compositions containing up to 20 at% Si. Compositions immediately beyond the boundaries to this region often yield part glassy, part crystalline foils on quenching. Such foils were characteristically brittle. In general, the glass forming region reported here closely corresponds to those reported by other investigators [2–5]. The differences are probably due to minor variations in melt quenching techniques. Binary Fe–Si glasses have only been produced by vapour deposition processes [9].

The ductility of Fe–B–Si glassy ribbon, measured in terms of the ribbon flexibility, is a function of both ribbon thickness and composition. For thicknesses of 20 μm or less, all ribbon produced could be bent back on itself without failure, yielding $\epsilon = 1$. As ribbon thickness was increased, compositional effects became apparent. The maximum ribbon thickness (in μm) for $\epsilon = 1$ bending is plotted as a function of composition in Fig. 4. The addition of Si to Fe–B alloys enhances ductility, especially for compositions along the eutectic trough. Ductile ribbon of maximum thickness is obtainable from eutectic compositions extending from $Fe_{80}B_{13}Si_7$ to $Fe_{78}B_{12}Si_{10}$.

## 5. Thermal stability

The onset of crystallization, $T_x$, of glassy Fe–B–Si alloys is shown in Fig. 5. The thermal stability of the system is clearly enhanced by the presence of

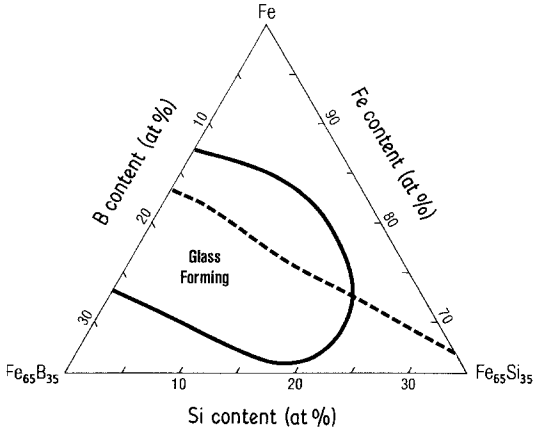


*Figure 3* The glass forming region of the Fe–B–Si composition diagram. The eutectic trough is marked by the dashed ( – – – ) line.

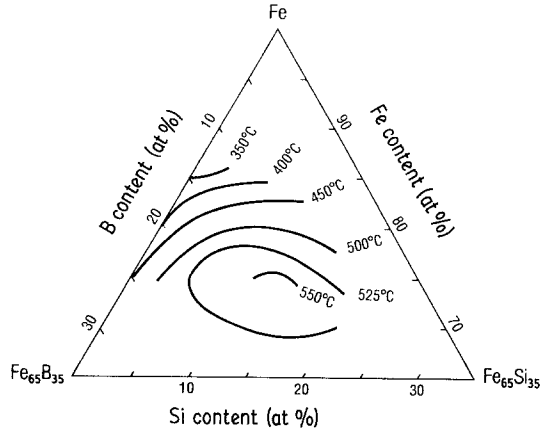


*Figure 5* Contours of constant $T_x$ (onset of crystallization) for glassy Fe–B–Si alloys, at 20° C $min^{-1}$ heating rate.

Si; replacing either Fe or B with Si increases $T_x$. A maximum $T_x$ of approximately 550° C occurs along an arc extending from $Fe_{75}B_{14}Si_{11}$ to $Fe_{74}B_{11}Si_{15}$.

The crystallization behaviour of metallic glass alloys of the family $Fe_{82}B_{18-x}Si_x$ has been studied in detail. The continuous heating transformation temperatures (at 5° C $min^{-1}$) as a function of composition are shown in Fig. 6. Glass transition temperatures prior to crystallization were not observed. Metallic glass alloys containing low Si concentrations (< 2 at%) devitrify directly to α-(Fe, Si) and tetragonal $Fe_3B$ in one step. At higher Si levels, a two step transformation occurs. As the sample is heated through the initial transformation temperature ($T_{x1}$), α-(Fe, Si) crystallites precipitate from the metallic glass. At a higher temperature ($T_{x2}$), the remaining glass crystallizes into α-(Fe, Si) and $Fe_3B$.

These results are analogous to those in the $Fe_{100-y}B_y$ system [1, 10]. In the binary system, hypereutectic glasses ($y \geqslant 18$) devitrify directly to α-Fe and $Fe_3B$ in one step. For hypoeutectic compositions ($y < 18$), two sequential transformations occur, as in the Fe–B–Si case: α-Fe precipitates forming at $T_{x1}$ with the remainder of the glass transforming to α-Fe and $Fe_3B$ at $T_{x2}$. In all cases, $Fe_3B$ is itself metastable and decomposes into α-Fe and $Fe_2B$ with further heating.

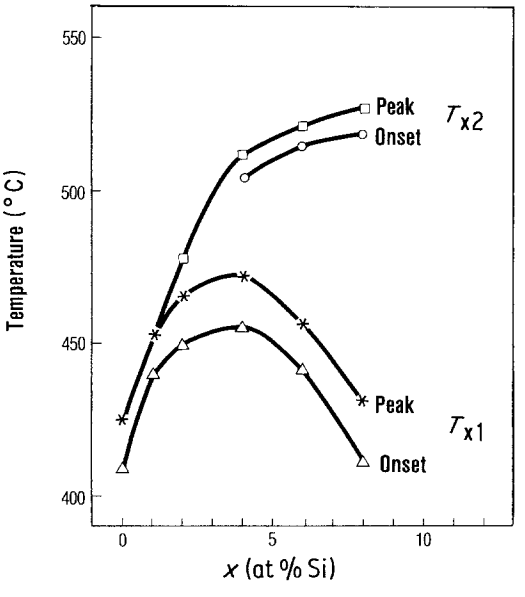


*Figure 6* Crystallization behaviour of glassy $Fe_{82}B_{18-x}Si_x$ alloys, at 5° C $min^{-1}$ heating rate. Temperatures for the onset of crystallization and peak crystallization rate are indicated.

## 6. Magnetic properties

The Curie temperature, $T_c$, measurements as a function of composition are shown in Fig. 7. In the low metalloid region, the addition of Si, replacing B or Fe, increases $T_c$. This increase, however, is less dramatic than the similar effect of Si on $T_x$. These results are equivalent to those reported by Luborsky *et al.* [2] for low Si alloys and Narita *et al.* for high Si compositions [4, 5].

The room temperature saturation magnetization, $\sigma_s$, has been reported in detail by Luborsky [2]. These data are transcribed onto a ternary composition diagram in Fig. 8. A ridge of maximum $\sigma_s$ extends from $Fe_{80}B_{20}$ to $Fe_{82}B_{12}Si_6$. Saturation magnetization drops sharply as composition is varied to higher or lower Fe content. The ridge of maximum $\sigma_s$ is skewed to the eutectic trough, intersecting it at approximately $Fe_{82}B_{15}Si_3$.

The coercive forces, $H_c$, of glassy Fe–B–Si ribbon samples were also determined by Luborsky [2]. These values, as a function of composition, are shown in Fig. 9a and b for as-cast and annealed samples, respectively. Unlike Curie temperature and saturation magnetization, the compositional dependence of the coercive force demonstrates a relationship to the eutectic composition. Both as-cast and annealed samples exhibit minimum $H_c$ at compositions along the eutectic trough.

## 7. Discussion

The relationship between eutectic phenomena and metallic glass formation in metal–metalloid

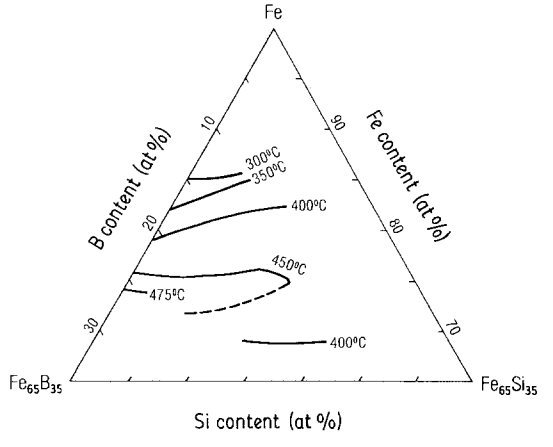


*Figure 7* Contours of constant Curie temperature for glassy Fe–B–Si alloys.

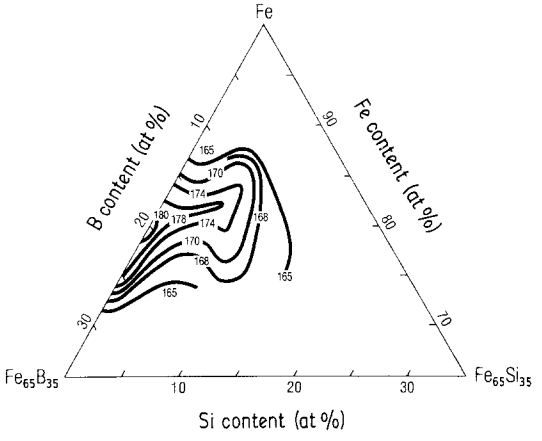


*Figure 8* Contours of constant saturation magnetization, in emu $g^{-1}$, for glassy Fe–B–Si [2].

alloys has long been recognized [11, 12]. Eutectic crystallization involves the diffusional separation of the constituent elements into regimes of specific crystallographic and stoichiometric nature. The kinetics of this microsegregation are relatively slow. Glass formation, which is dependent on the suppression of solidification by crystallization, is therefore most readily accomplished at a eutectic.

This concept is clearly supported in the Fe–B–Si system. The glass forming region closely follows the eutectic trough [L → α (Fe, Si) + $Fe_2B$] across the ternary composition diagram. In addition, the thickest ductile sections of metallic glass, reflecting relative ease of formation, occur at compositions along the eutectic trough as, also, do the maximum crystallization temperatures, reflecting the thermal stability of the glasses formed.

Although the compositional dependence of the ferromagnetic properties of metallic glass alloys, including Fe–B–Si, has been studied in detail, no attempt has been made to correlate these properties to the eutectic phenomena. Curie temperature and saturation magnetization behaviour have been explained in terms of short range structural effects influenced by the equilibrium crystal structures [1]. However, no direct evidence of the occurrence of such structures exists, nor is any relationship between $T_c$ and $\sigma_s$ and the eutectic phenomena evident.

On the other hand, the coercive forces in glassy Fe–B–Si bear a distinct relationship to the eutectic phenomena. Fig. 9a and b illustrate that minimum values of $H_c$ occur at compositions along the eutectic trough, with $H_c$ increasing rapidly as the alloy chemistry is varied to hypo- or hypereutectic compositions. This behaviour implies variations in atomic structure, internal stress state or both as the metallic glass composition is varied away from the eutectic.

Eutectic liquids, and the metallic glass structures derived from them, are believed to possess unique structures characterized by distinct short range ordering [11]. The existence of such structure in eutectic Fe–B–Si glasses would certainly influence $H_c$. To be consistent with the observed minima in $H_c$, one would expect that glasses be more homogeneous in composition and stress distribution at the euetectic, thereby offering relatively little resistance to magnetic domain wall motion.

A near-eutectic composition is also desirable from the standpoint of ease in production and processing. The low viscosity of a eutectic liquid

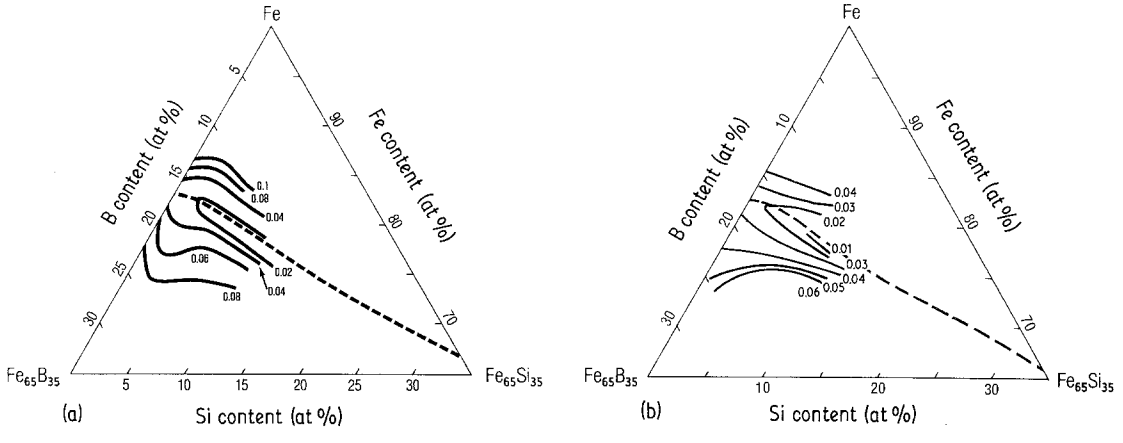


*Figure 9* Contours of constant coercive fields, in Oe, for (a) as-cast and (b) annealed glassy Fe–B–Si alloys [2]. The eutectic trough is marked by the dashed ( – – – ) line.

results in more uniform ribbon geometry. This yields more efficient packing of the glass ribbon, critical in most magnetic applications. The reduced liquidus temperature permits lower casting temperatures resulting in less wear on the casting nozzle and substrate.

## 8. Summary

The equilibrium solidification behaviour of Fe-rich Fe–B–Si alloys has been defined. A eutectic trough extends from the binary eutectic on the Fe–B edge of the ternary composition diagram towards the binary eutectic on the Fe–Si edge. The glass forming region in this system closely follows the course of the eutectic trough across the ternary diagram, extending from the Fe–B edge to ternary compositions containing up to 20 at % Si. Maximum glassy metal ribbon thickness and crystallization temperature and minimum coercive force are associated with compositions along the eutectic trough.

## References

1. R. HASEGAWA and R. RAY, *J. Appl. Phys.* **49** (1978) 4174.
2. F. LUBORSKY, J. BECKER, J. WALTER and H. LIEBERMANN, *IEEE Trans. Magn.* **MAG-15** (1979) 1146.
3. K. HOSELITZ, *J. Magnet. Magnet. Mater.* **20** (1980) 201.
4. F. K. NARITA, H. FUKUNAGA, J. YAMASAKI and K. HARA, *ibid.* **19** (1980) 145.
5. F. K. NARITA, H. FUKUNAGA, J. YAMUSAKI and K. HARA, *Supplement Sci. Rep. RITU,* **A.** (1980) 251.
6. R. HASEGAWA, R. C. O'HANDLEY and L. L. MENDELSOHN, *AIP Conf. Proc.* **34** (1976) 298.
7. R. C. O'HANDLEY, C. P. CHOU and N. DeCRISTOFARO, *J. Appl. Phys.* **50** (1979) 3603.
8. F. LUBORSKY, P. FRISCHMANN and L. L. JOHNSON, *J. Magnet. Magnet. Mater.* **8** (1979) 318.
9. G. MARCHAL, Ph. MANGIN and C. JANOT, *Solid State Comm.* **18** (1976) 739.
10. J. L. WALTER, S. F. BARTRAM and I. MELLA, *Mater. Sci. Eng.* **36** (1978) 193.
11. J. J. GILMAN, *Phil. Mag. B.* **37** (1978) 577.
12. H. J. V. NIELSEN, *Z. Metallk.* **70** (1979) 180.

*Received 2 November 1981*
*and accepted 18 January 1982*